

Learning Rank Reduced Interpolation with Principal Component Analysis

Matthias Ochs¹, Henry Bradler¹ and Rudolf Mester^{1,2}

Abstract—In computer vision most iterative optimization algorithms, both sparse and dense, rely on a coarse and reliable dense initialization to bootstrap their optimization procedure. For example, dense optical flow algorithms profit massively in speed and robustness if they are initialized well in the basin of convergence of the used loss function. The same holds true for methods as sparse feature tracking when initial flow or depth information for new features at arbitrary positions is needed. This makes it extremely important to have techniques at hand that allow to obtain from only very few available measurements a dense but still approximative ‘sketch’ of a desired 2D structure (e.g. depth maps, optical flow, disparity maps, etc.).

The 2D map is regarded as sample from a 2D random process. The method presented here exploits the complete information given by the principal component analysis (PCA) of that process, the principal basis *and* its prior distribution. The method is able to determine a dense reconstruction from sparse measurement. When facing situations with only very sparse measurements, typically the number of principal components is further reduced which results in a loss of expressiveness of the basis. We overcome this problem and inject prior knowledge in a maximum a posteriori (MAP) approach.

We test our approach on the KITTI and the virtual KITTI datasets and focus on the interpolation of depth maps for driving scenes. The evaluation of the results show good agreement to the ground truth and are clearly better than results of interpolation by the nearest neighbor method which disregards statistical information.

I. INTRODUCTION

This paper addresses the task of computing a dense reconstruction of depth images as they are typically of interest in visual odometry and SLAM. This task is challenging if only a very sparse measurement of the depth is given. We focus on the situation where depth (or disparity) information is available for less than 1/1000 of all pixels (e.g. for about 200 pixels for an image of size 1240×370). As we will see, it is possible to tackle this problem successfully if a suitable statistical model exists for the regarded class of depth images.

It may seem surprising that this problem can be addressed using a Bayesian version of PCA. Determining a PCA model offers *two* powerful approaches: 1) reducing the rank of the model (subspace model) 2) using the eigenvalues of the initial processes covariance matrix reflected in the variances of the PCA model.

In this paper we demonstrate how to overcome this indeterminacy by including prior knowledge about the principal components which is already given by the PCA. We

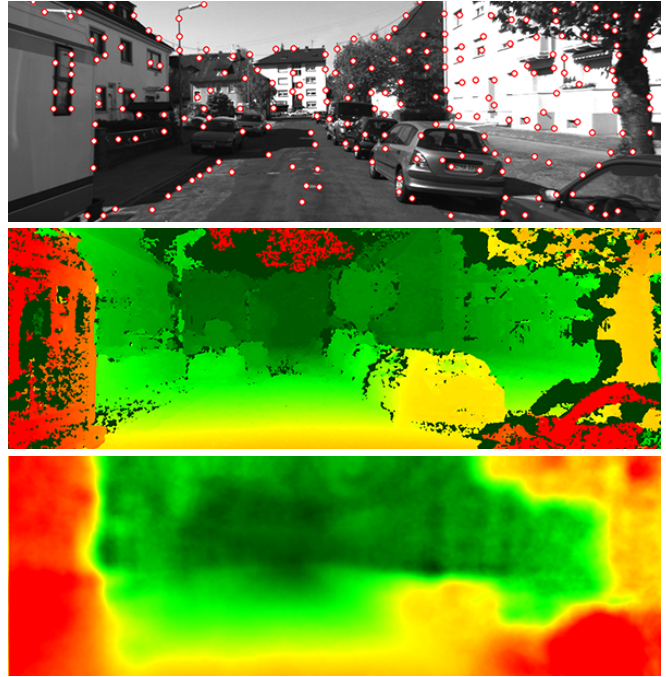


Fig. 1: The top image shows frame 532 of the KITTI test sequence 19 and indicates where sparse measurements of the depth have been obtained (circles). The middle image shows, as reference, a SGBM depth map. Our interpolation of the sparse measurements is presented at the bottom.

determine a best set of coefficients for a representation in the principal coordinate system by utilizing a maximum a posteriori estimation (MAP). Furthermore, we demonstrate how this approach can be used to get a dense reconstruction of data for which only very sparse information is available and which though preserves the coarse structure and the main print of the dense original data.

The structure of this paper is as follows. In the approach part we show how to learn the basis of principal components for a specific class of data. In our case we deal with depth maps for an application in an automotive scenario, but of course the method is not limited to this exemplary case. For a sparse measurement, we then derive the best representation in a given PCA basis from a statistical approach which exploits prior knowledge about the general distribution of the principal components. The interpolation step consists of a transformation from the principal coordinate system back to the system of the original data. This finally yields the dense reconstruction sought.

¹Visual Sensorics & Information Processing Lab, Goethe University, Frankfurt am Main, Germany

²Computer Vision Laboratory, ISY, Linköping University, Sweden

In the experimental part, we evaluate our approach on two familiar datasets. We regard the well known KITTI odometry dataset [1] and the more recent synthetic *Virtual KITTI* dataset [2]. The latter has the benefit of providing pixelwise ground truth of the depth structure. We investigate also the applicability of our approach by comparing the reconstructed 3D point cloud and pixel correspondences (stereo for KITTI / temporal for Virtual KITTI) against reference values (SGBM for KITTI / groundtruth for Virtual KITTI). The pixelwise evaluation of our dense interpolation shows very good results and that it is clearly superior to interpolations which do not make use of statistical approaches as, e.g., nearest neighbour interpolation. An example of dense reconstruction obtained by our method is shown in figure 1.

II. RELATED WORK

Monocular visual odometry / SLAM algorithms became more and more popular recently for perception of the environment in autonomous driving. All those algorithms have in common that their performance is strongly dependent on a good initialization of the relative pose and feature points between two consecutive frames. Engel et al. [3] proposed in their LSD-SLAM approach a randomly generated depth map, which is improved with valid measurements and propagated during tracking with key frames. A similar approach is pursued by Forster et al. [4]. They maintain the depth maps for initialization with Bayesian depth filters and matching desired feature points. The authors of the propagation based tracking method [5] initialize new feature points based on the displacements computed by phase correlation. The depth values of feature points that have been tracked at least once before are propagated into the next frame, using epipolar matching, an initial estimate of the next relative pose and a subsequent joint optimization of this pose and the point correspondences [6].

All these monocular SLAM methods have in common that they only reconstruct a sparse set of points. For autonomous driving, it is obviously not sufficient to have 3D information only at some few points — densification is necessary. In order to allow a densification process to converge quickly into a true detailed dense map, it is useful to have a solid method that generates initial estimates of these dense depth maps.

Also for many dense optical flow methods [7], [8], it is advantageous to have a good initialization for the dense depth map, since computationally expensive variational approaches converge faster if they are initialized close to the optimum.

Since estimating a depth map or an optical flow field is almost the same for rigid scenes and a given relative pose, we compare our method also to related work in the field of optical flow estimation.

There are dense optical flow methods which also use sparse measurements for initialization. For example, Gibson and Span [9] uses a sparse feature tracking algorithm in their first stage. In their second step, a traditional dense optical flow optimization is followed. SIFT Flow [10] uses densely sampled SIFT features, which are matched between

two images. These matches are then used to compute a dense optical flow field. Leordeanu et al. [11] also used sparse measurements to initialize their dense optical flow method. They use a sparse set of correspondences to perform a sparse-to-dense interpolation which are then refined using a total variation model. Wulff and Black [12] also calculate dense optical flow given a set of sparse feature point matches. These points are used to estimate several PCA flow field layers. The combination of these layers into a dense optical flow field is done with an MRF. This approach is very similar to our PCA interpolation of depth maps. In contrast to them, we use a maximum a-posteriori estimation to estimate weighted linear combination of the PCA basis. This leads to significantly better interpolated depth maps.

Robert et al. [13] estimate the optical flow field and the ego-motion based on a probabilistic PCA. This approach is extended in the work by Herdtweck and Curio [14] into the so-called 'expert models'. Each of those expert models represents a specific pre-trained subspace of the training data. The optical flow field and ego-motion are estimated by an expert system and an outlier model. Another learning-based method for estimating a depth map are proposed by Saxena et al. [15]. They learn discriminatively a Markov Random Field at multiple spatial scales to predict depth maps.

Besides all those 'classical' computer vision approaches, there also exists methods that compute depth maps or optical flow fields with deep learning networks. Eigen et al. [16] presented one of the first works which use deep learning to estimate depth maps. This approach was improved and extended to compute surface normals and also semantic labels in [17]. All these deep learning techniques have the disadvantage that they need a huge amount of precise ground truth data for training. Garg et al. [18] proposed an unsupervised framework to train a CNN for estimation of a depth map from a single image without the need of annotated ground truth depths. Another drawback of the deep learning networks has recently been solved by Mancini et al. [19]. They included a *long short term memory* into their network. By this, it is possible to estimate the global scale of the depth maps. Previously, this was a problem since a deep network was only capable to estimate a unscaled depth map from a monocular images.

III. APPROACH

Our densification / interpolation scheme consists of the following three steps:

- learning a basis (once for a specific class of data)
- projection to this basis (once for each sparse measurement)
- interpolation by projection back to original basis (once for each sparse measurement)

The first step only has to be performed once for each class of data considered. Thus, we need to learn one basis which is suitable to represent depth maps as they are typically observed in an automotive driving scenario [1], [20]. This learning step can be done offline, utilizing a large training data set (like the depth data of the complete KITTI dataset)

that represents the typical statistics of the data to be expected in use.

Given this precomputed basis, any set of sparse measurement data needs to be associated with the coefficients of the basis such that the linear superposition of the basis vector (=basis images) complies with the sparse measured data, either perfectly, or as good as possible in the sense of a suitable metric. In our scenario, the number of basis vectors will, in general, by far exceed the number of measurements (underdetermined problem). This is not a problem as long as we include prior knowledge about the coefficient distribution. We show that this prior knowledge is already available from the learning step. This is similar to the approach of [12].

Finally, the representation of the sparse measurement in the learnt basis is used to transform the coefficients back to the original domain. This gets a dense interpolation.

Note: When using the word *depth* in this paper, we generally mean a quantity which is suitable to express the depth. E.g., this also applies for the inverse depth or disparity which both possesses advantages over the actual depth when it comes to statistical properties and numerical representation. If depth is encoded as disparity, the conversion factor (depends on focal length and base of a stereo setup) to inverse depth must be given. Even though disparity in general is used in stereo scenarios, it can be numerically beneficial to store depth or inverse depth as disparity in a non stereo setup by choosing a reference stereo base for conversion.

A. Learning a Basis via PCA

We start with a training set of n depth maps $\vec{d}_i \in \mathbb{R}^s$, each of dimension s , which cover the typical range variation which could be expected in the scenario. In our case of high-resolution depth maps the number of training samples is much smaller than their dimension $n \ll s$. Thus, at most n of the potential s degrees of freedom of the data can be revealed. However, for images of a specific class (e.g. depth maps), in contrast to random permutations, already a few principal components are sufficient to express the coarse impression and the main information of the image.

To find these significant degrees of freedom, we employ PCA on the training set. For that purpose, the mean and covariance need to be computed. The unbiased sample mean and covariance of the training set are given by:

$$\vec{m} = \frac{1}{n} \sum_{i=0}^{n-1} \vec{d}_i, \quad (1)$$

$$\mathbf{C} = \frac{1}{n-1} \mathbf{D} \cdot \mathbf{D}^T \in \mathbb{R}^{s \times s}, \quad \text{with} \quad (2)$$

$$\mathbf{D} = \begin{pmatrix} \vec{d}_0 - \vec{m}, \dots, \vec{d}_{n-1} - \vec{m} \end{pmatrix} \in \mathbb{R}^{s \times n}. \quad (3)$$

The spectral decomposition of the covariance yields

$$\mathbf{C} = \mathbf{U} \cdot \text{diag}(\lambda_0, \dots, \lambda_{s-1}) \cdot \mathbf{U}^T, \quad (4)$$

$$\mathbf{U} = (\vec{u}_0, \dots, \vec{u}_{s-1}) \in \mathbb{R}^{s \times s}, \quad (5)$$

with the principal components and the corresponding variances stored as basis vectors \vec{u}_i in the columns of \mathbf{U} and

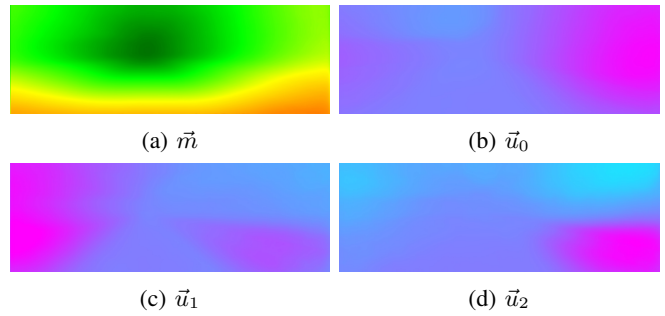


Fig. 2: Mean depth and the three most significant basis vectors computed via the PCA of the depth maps of all KITTI training sequences (00-10).

as eigenvalues in descending order in the diagonal matrix $\text{diag}(\lambda_0, \dots, \lambda_{s-1})$, $\lambda_0 \geq \dots \geq \lambda_{s-1}$, respectively. So, for a given depth map \vec{d} the basis coefficients \vec{y} of the principal coordinate system are

$$\vec{y} = \mathbf{U}^T \cdot (\vec{d} - \vec{m}), \quad \vec{d} = \mathbf{U} \cdot \vec{y} + \vec{m}. \quad (6)$$

From equation (2) it becomes obvious that \mathbf{C} is rank deficient, $\text{rank}(\mathbf{C}) \leq n \ll s$, and since the sample covariance is computed using the sample mean we even know $\text{rank}(\mathbf{C}) < n$ or rather $\lambda_{i \geq (n-1)} = 0$. This implies that the PCA of the training set allows to uncover at most $n-1$ degrees of freedom, the mean and $n-2$ principal components which encode information (nonzero variance).

However, for our aim of a coarse but dense interpolation, we do not need a complete basis of principal components. If we examine the cumulative sum of the variances λ_i (see figure 7), a reasonable limit l of basis vectors to consider can be determined. We restrict ourselves to a basis that consists of the $l \ll n \ll s$ most important basis vectors that are capable of explaining more than 90% of the information (variance) of the training set. All depth maps \vec{d} of the same class as the training samples possess a sufficiently good approximation in this *truncated basis*.

$$\mathbf{B} = (\vec{u}_0, \dots, \vec{u}_{l-1}), \quad (7)$$

$$\mathbf{\Lambda} = \text{diag}(\lambda_0, \dots, \lambda_{l-1}). \quad (8)$$

Figure 2 shows an example of the mean depth and the most significant principal components.

B. Projection to the Principal Coordinate System

How do we find the coefficients \vec{y} that are most suited to express a sparse measurement $\tilde{\vec{z}} = \vec{d} - \tilde{\vec{m}}$ (the tilde denotes that only some few components of the vector are given)?

In our application, we face a situation where the number of measured components of the depth map is even below the size l of our reduced basis \mathbf{B} . In this case a simple (weighted) least squares approach to compute the coefficient vector \vec{y} via the minimization of the difference of measured and reconstructed signal would lead to an under-determined problem. We take care of this by including prior knowledge about the

coefficients which is already given by the eigenvalues $\mathbf{\Lambda}$ of the sample covariance \mathbf{C} .

This leads to a maximum a posteriori (MAP) estimation of \vec{y} , where the maximization of the posterior,

$$p(\vec{y} | \vec{z}) = \alpha \cdot p(\vec{z} | \vec{y}) \cdot p(\vec{y}) \rightarrow \max, \quad (9)$$

is equivalent to the minimizing of its negative logarithm

$$-\log(p(\vec{y} | \vec{z})) = \alpha' + (\vec{z} - \tilde{\mathbf{B}} \cdot \vec{y})^T \cdot \mathbf{C}_{\vec{z}}^{-1} \cdot (\vec{z} - \tilde{\mathbf{B}} \cdot \vec{y}) + \vec{y}^T \cdot \mathbf{C}_{\vec{y}}^{-1} \cdot \vec{y} \rightarrow \min. \quad (10)$$

The variables α and α' in equation (9) and (10) collect all terms independent of \vec{y} . The prior covariance is given by the eigenvalues of the sample covariance $\mathbf{C}_{\vec{y}} = \mathbf{\Lambda}$ and the measurement covariance is assumed to be uncorrelated and to possess constant variance for all components of the measurement $\mathbf{C}_{\vec{z}} = \sigma_z^2 \cdot \mathbf{I}$.

In terms of the posterior, the estimate $\hat{\vec{y}}$, defined by the linear equation system

$$\left(\sigma_z^2 \cdot \mathbf{\Lambda}^{-1} + \tilde{\mathbf{B}}^T \cdot \tilde{\mathbf{B}} \right) \cdot \hat{\vec{y}} = \tilde{\mathbf{B}}^T \cdot \vec{z}, \quad (11)$$

gives the best representation of the sparse measurement \vec{d} in the PCA coordinate system. Its covariance is given by

$$\text{Cov}[\hat{\vec{y}}] = \left(\sigma_z^2 \cdot \mathbf{\Lambda}^{-1} + \tilde{\mathbf{B}}^T \cdot \tilde{\mathbf{B}} \right)^{-1}. \quad (12)$$

C. Dense Interpolation

Once we computed the coefficient vector estimate $\hat{\vec{y}}$ via the MAP approach, it is straightforward to get the estimate of the reconstructed full depth map \hat{d} to the sparse measurement \vec{d} :

$$\hat{d} = \mathbf{B} \cdot \hat{\vec{y}} + \vec{m} \quad (13)$$

$$\text{Cov}[\hat{d}] = \mathbf{B} \cdot \text{Cov}[\hat{\vec{y}}] \cdot \mathbf{B}^T \quad (14)$$

$$\approx \sum_{i=0}^{l-1} \kappa_i^2 \cdot \vec{u}_i \cdot \vec{u}_i^T. \quad (15)$$

In equation (15), we ignored all possible correlations of $\hat{\vec{y}}$ and only considered the diagonal elements κ_i^2 of $\text{Cov}[\hat{\vec{y}}]$ to get an approximation of the covariance of the reconstruction. Furthermore, we define the uncertainty image $\vec{\xi}$ that consists of the diagonal elements of the approximated covariance as

$$\vec{\xi} = \text{diag} \left(\sum_{i=0}^{l-1} \kappa_i^2 \cdot \vec{u}_i \cdot \vec{u}_i^T \right). \quad (16)$$

Apart from the approximations made in equation (15) and (16), the uncertainty image $\vec{\xi}$ is the propagation of the combined uncertainty of the data (likelihood) and the prior term of the MAP approach to the original image domain of the depth map.

IV. EXPERIMENTS

The evaluation of our method is performed on all 11 test sequences of the KITTI odometry benchmark [1] and on the 5 synthetic sequences of the Virtual KITTI dataset [2], which provides ground truth depth information on pixel level. We evaluate our estimated depth map in terms of 2D and 3D projection errors and only for valid points. This means, that only points are taken into account which are in the field of view of the camera after projection them from frame A to another frame B and valid ground truth data exists. During all our experiments, we set the measurement noise to $\sigma_z = 2$ px.

Furthermore, we compare our results with the nearest neighbor interpolation for the same sparse data points. Finally, in a further experiment, our approach uses the depth values of sparse discrete feature points from a state-of-the-art monocular SLAM algorithm [5]. This demonstrates that dense interpolated depth maps can be computed with sparse measured depth values in practice.

A. Learning the PCA Basis

For the offline learning of the PCA basis, we use the 10 training sequences of the KITTI odometry benchmark [1]. This dataset consists of 23201 images, which is equal to the number of our learned PCA basis vectors. We do not use the training set for optical flow or stereo benchmark, because these datasets consists only of few images and sparse ground truth depth from a LIDAR scanner; this does not provide enough data and enough variation to learn the PCA basis.

Unfortunately, the ground truth depth information is not available for the odometry benchmark. Thus, we computed the depth maps with the semi-global block matching (SGBM) algorithm by Hirschmüller [21]. Note that we are using disparity values for all depth maps listed below. Due to stereo ambiguities, stereo shadows and regions where SGBM cannot find a match, these depth maps typically contain a number of known invalid pixels. Since the PCA basis should not be trained with such invalid regions, we have interpolated these regions with a standard nearest neighbor interpolation. Furthermore, we used a 5×5 box filter to blur the depth maps, because we cannot expect the stochastic PCA model to represent fine structured elements in the depth field.

Finally, the PCA basis has been learned on 23201 depth maps. Hence, the complete PCA basis consists of 23201 eigenvalues and eigenvectors. In the following, for reasons of computational effort, we use only the 500 largest eigenvalues and their corresponding eigenvectors. This allows us to reconstruct approximately 95% of the information within a depth map.

B. Evaluation Measures

The estimated depth maps are evaluated through the experiments based on the 2D and 3D projection errors as evaluation measures. Since we used disparities d as depth values for learning the PCA basis, and since both the baseline b and the focal length f of the underlying stereo camera is known, the actual depth w is derived from $w = \frac{b \cdot f}{d}$.

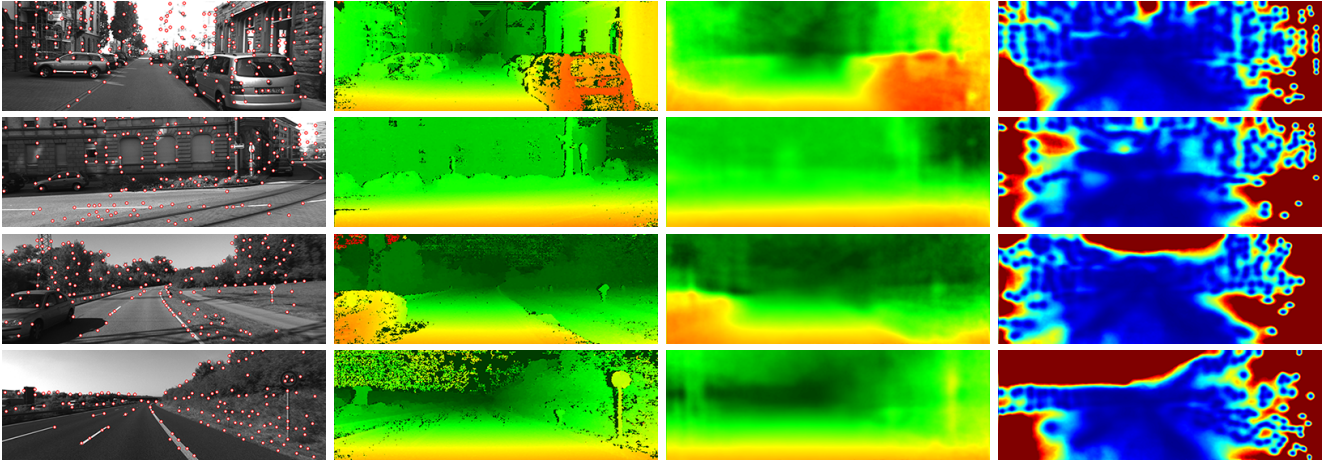


Fig. 3: Example results of the KITTI dataset with different driving scenes (urban, rural, highway). The first column shows the selected feature points. The SGBM depths (second column) are used at these locations to interpolate the depth maps with our approach (third column). The uncertainty image of our interpolation is shown in the last column (dark red implies high uncertainty).

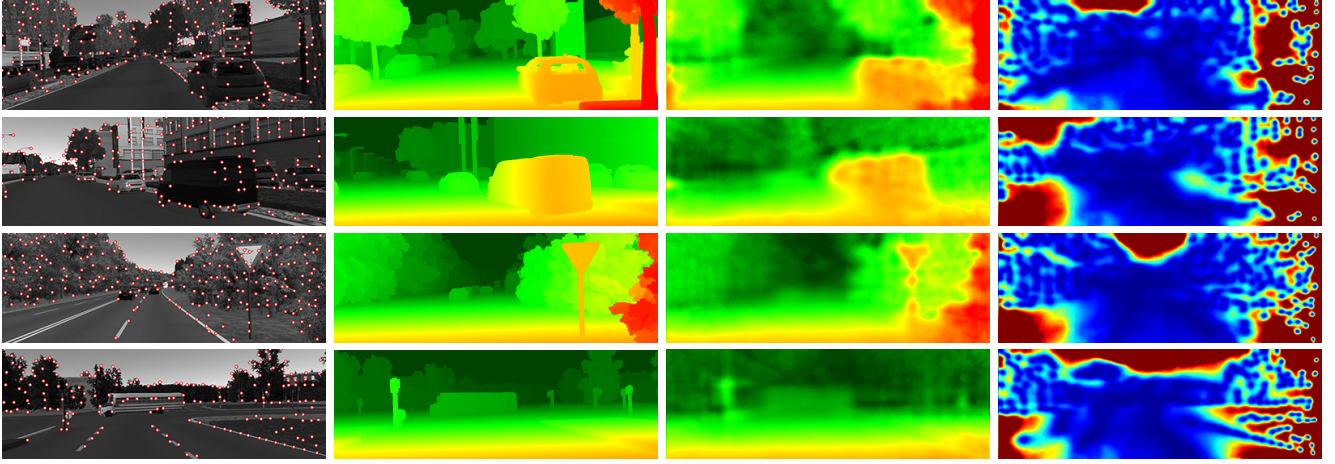


Fig. 4: Example results of the Virtual KITTI dataset with different driving scenes (urban, rural). The first column shows the selected feature points. The ground truth depth are presented in the second column. These depth values are used at detected pixel locations to interpolate the depth maps with our approach (third column). The uncertainty image of our interpolation is shown in the last column (dark red implies high uncertainty).

Given a 2D image point \vec{x} and the known camera matrix \mathbf{K} , the corresponding 3D point \vec{X} can be computed as:

$$\vec{X} = w \cdot \mathbf{K}^{-1} \cdot \begin{pmatrix} \vec{x} \\ 1 \end{pmatrix}. \quad (17)$$

A 3D point \vec{X}_A in frame A can be projected into another frame B with a given projection matrix $\mathbf{P} \in \mathbb{R}^{4 \times 4}$ using the following equation:

$$\begin{pmatrix} \vec{X}_B \\ 1 \end{pmatrix} = \mathbf{P} \cdot \begin{pmatrix} \vec{X}_A \\ 1 \end{pmatrix}. \quad (18)$$

The re-projection of a 3D point \vec{X} into the image coordinate system with the camera matrix \mathbf{K} is given by the projection operation $\pi(\cdot)$.

For an arbitrary image point in frame A , a reference 3D point $\vec{X}_{A,ref}$, where the depth is obtained by ground truth

data, and an estimated 3D point $\vec{X}_{A,est}$ given the interpolated depth is computed. These two 3D points are projected into frame B . The two evaluation measures are then defined as follows:

$$\Delta_{3D} = \|\vec{X}_{B,ref} - \vec{X}_{B,est}\|_2^2 \quad (19)$$

$$\Delta_{2D} = \|\pi(\vec{X}_{B,ref}) - \pi(\vec{X}_{B,est})\|_2^2. \quad (20)$$

Hence, the 3D error Δ_{3D} measures the deviation between the projected ground truth 3D point and the estimated one. The 2D error Δ_{2D} is a measure for the mismatch of a projected point into the image B from the ground truth position of the true position in the image.

C. KITTI Dataset

The KITTI odometry test dataset [1] contains 11 sequences with more than 29000 images, which show different scenes

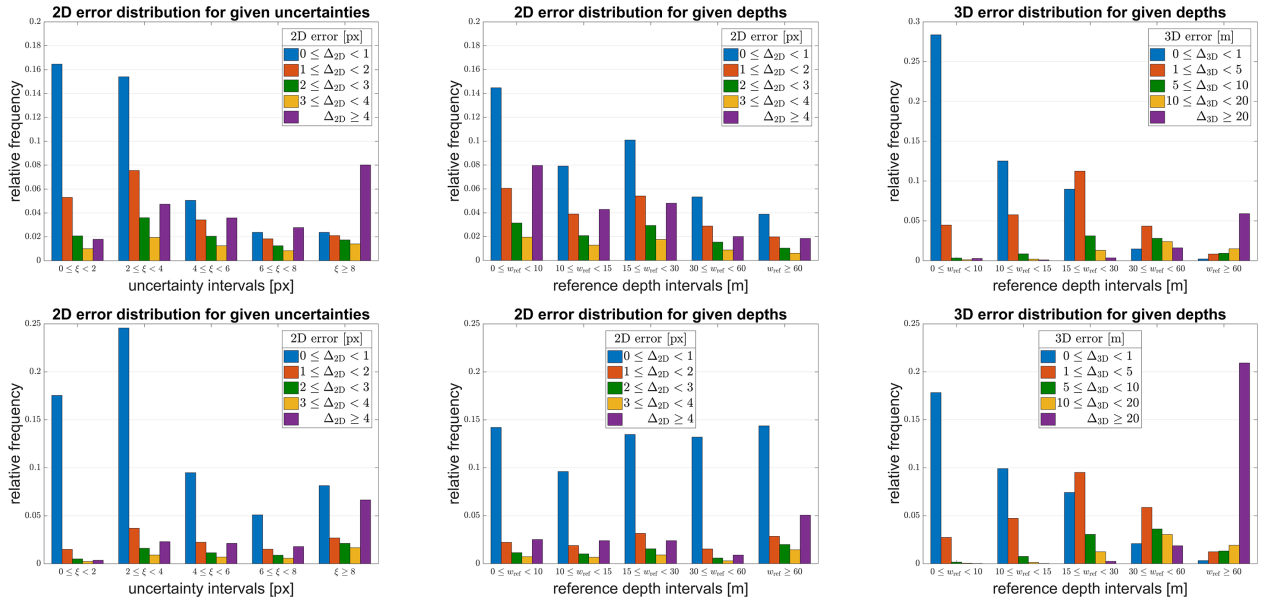


Fig. 5: In the first row, the evaluation is performed on the KITTI dataset. The second row shows the same evaluations metrics on the Virtual KITTI dataset. The 2D error Δ_{2D} distribution for different uncertainty levels are shown in the first column. In the second and the third column, the 2D error Δ_{2D} respectively the 3D error Δ_{3D} exhibits the distributions for different depth bins.

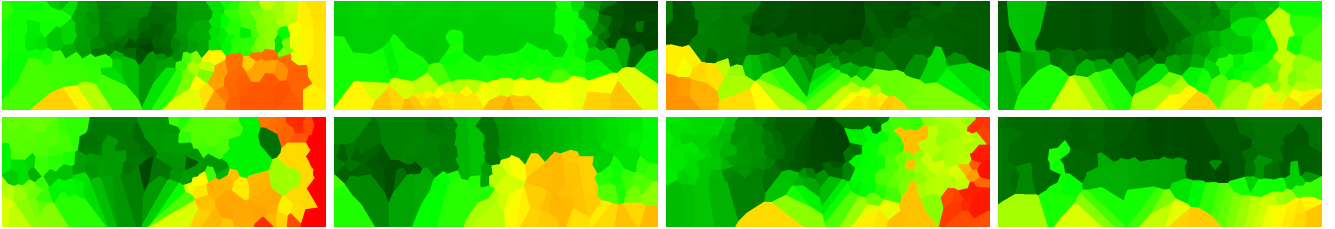


Fig. 6: Nearest neighbor interpolation based on the same data points, which are used for the PCA based interpolation in figure 3 and 4. The first row correspond to the KITTI dataset examples and the second to the VKITTI ones.

like driving on urban, rural, or highway roads. This variety of scenes is challenging for our method, because the learned PCA basis must represent all these unseen scenes.

Since KITTI does not provide the ground truth projection parameters between two consecutive temporal frames, we cannot evaluate our approach temporally. Therefore we used the known stereo projections and evaluate our method only between the two cameras of the stereo system. This does not mean that our method is limited to stereo. It depends only on a sparse set of depth measurements. For generating such a set, we use the ‘good features to track’ algorithm by [22]. The depth values for each detected feature point are obtained by the depth map which is computed by SGBM. Examples of the detected feature points and the SGBM depth maps are shown in the first and second column in figure 3.

Even though we have a small basis of only 500 eigenvectors, it is possible to reconstruct quite well from only a few measurements as long as they are distributed reasonably across the image. Some interpolation examples are shown in the third column of figure 3. In the corresponding uncertainty images $\vec{\xi}$ (last column), it can be seen that our

interpolation method is uncertain in regions where nearly no measurements located, like in the sky. Thus, the uncertainty can serve as a measure how good the depth can be estimated without knowing the ground truth. This assumption is also supported by the first histogram in figure 5. The 2D error Δ_{2D} is relative small in the first bins and increases with the uncertainty intervals. However, more than 60% of all evaluated points from the datasets fall into the first two bins, which indicates that the uncertainty images as well as the interpolated depth maps perform well.

The other two histograms in the first row of figure 5 reveals that the errors of Δ_{2D} and Δ_{3D} are small, when the points are close to the camera. Not surprisingly, if the points are far away, the errors usually increase.

D. Virtual KITTI Dataset

We have evaluated our approach on all five public available sequences of the Virtual KITTI dataset [2] as well, which comprises driving scenes on urban and rural roads. We take all 2359 synthetic generated images and use ‘overcast’ as weather category. The learned PCA basis is the same like in

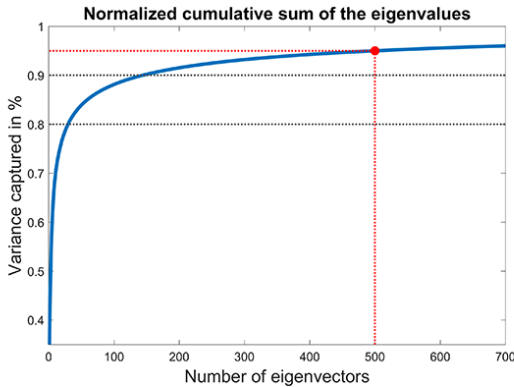


Fig. 7: The relative cumulative sum shows how much variance of the learnt depth map can be reconstructed by using a certain number of the largest eigenvalues and their corresponding eigenvectors.

the previous KITTI experiment. Thus, we have not learned a specific basis for VKITTI, which also shows the ability of generalization. However, the quantitative and qualitative results remained the same or are even better. The reason for this is probably the exact ground truth at pixel level. In contrast to the KITTI dataset, where we used the computed SGBM depth map as ground truth, VKITTI provides exact depth maps and poses. Another advantage is that we do not get wrong depth measurements for the interpolation. This could happen at the KITTI dataset, if a pixel location was selected where SGBM returned a false depth value. This may lead to a possibly bad representation in terms of the basis coefficients.

Due to presence of ground truth pose files and the non existence of stereo images in VKITTI, we evaluate our method in temporal direction (mono case). This implies that we use the available ground truth pose to project the feature points from frame A at time t to frame B at time $t + 1$. We use the same GFTT feature detector as in the KITTI dataset. In figure 4, some exemplary results are shown including the ground truth depth map of VKITTI and the uncertainty image of our interpolated depth map.

For all images of the VKITTI dataset, the 2D error Δ_{2D} of most image points falls into the first error interval, which means that $\Delta_{2D} < 1\text{px}$. This is independent of the uncertainty or depth intervals, as it is shown by the second row of figure 5. So, the estimated depth values are very close to the ground truth data on nearly all possible points. There are hardly any outliers. Additionally, if only the first two uncertainty intervals are used, more than 50% of the points are captured. Roughly 80% of these points are estimated with a deviation to the ground truth with less than 1 pixel.

The 3D error Δ_{3D} is small for points which are close to the camera. But there are also a large number of points in the far-field, where the error is quite large. This can be explained by the ground truth depth maps from VKITTI. They have limited the maximum distance to the camera at 655.35 meters. This is not equal to the KITTI dataset, where

the maximum distance is greater. Thus, the far-field points can be estimated with our learned PCA basis further away than it is encoded in the VKITTI depth maps, which leads to a significant error for points in the far field.

E. Comparison to Nearest Neighbor Interpolation

In this section, we compare our method to the nearest neighbor interpolation. For both methods, we use the same data points, of course. Figure 6 shows the nearest neighbor interpolation for the data, which we used for the examples in the KITTI and VKITTI experiments. In comparison to our method, the nearest neighbor interpolation is much coarser. Thus, the depth impression is not as good as in our method. This also exhibits the evaluation of the 2D error Δ_{2D} throughout both datasets. In the first two bins of the histogram 8, where $\Delta_{2D} < 2$, more points of our methods than from the nearest neighbor interpolation satisfy this condition. Additionally, in the last interval, where the 2D error is greater than 4 pixels, more points of the nearest neighbor interpolation are accumulated than from our approach.

Moreover, the mean of the 2D error Δ_{2D} for the nearest neighbor interpolation within both datasets is nearly 50% as larger compared to our interpolation. For the KITTI dataset, the mean value for the PCA method is 3.4 px and for the nearest neighbor 5.4 px. Similarly, the mean value for the VKITTI dataset is 2.0 px for our approach and 3.3 px for the other one.

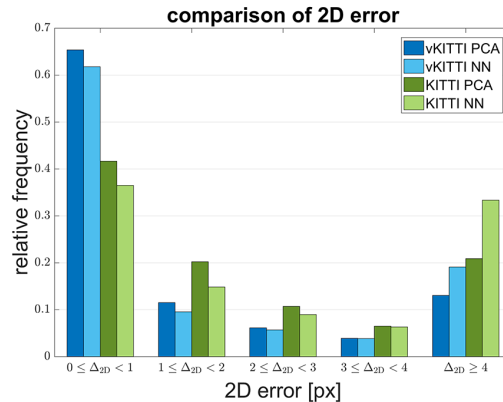


Fig. 8: Distribution of the 2D error Δ_{2D} for our approach and the nearest neighbor interpolation throughout both evaluated dataset.

F. PCA Interpolation in Practice

During all experiments so far, we used as sparse measurements always ground truth depth values. For the KITTI dataset, the SGBM depth values acted as ground truth values. However, these depth measurements are not correct in all cases either. Nevertheless, our method should also work with sparse data from a state-of-the-art monocular SLAM method.

Two exemplary results of a dense PCA interpolation with the sparse depth values from the propagation based tracking (PbT) algorithm [5] as input measurements are shown in

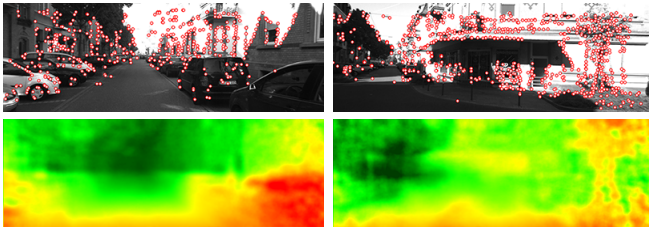


Fig. 9: Exemplary results of the dense PCA interpolation with sparse measurements using the monocular SLAM algorithm from [5].

figure 9. These examples come from the sequence 13 of the KITTI odometry test dataset [1]. The PbT method measures in these two frames roughly 400 feature points, which are represented in the first row of figure 9. Based on these sparse measurements, our PCA interpolation computes a dense depth map, which is shown in the second column of the same figure. These examples demonstrate that our interpolation is not limited to depth measurements which come from ground truth data. The depth impression of the interpolated depth map is coherent for non ground truth depths values, too. Hence, these computed dense depth maps can be used in practice for initialization purposes for dense matching or tracking approaches, like also claimed in [12].

V. SUMMARY & CONCLUSION

In this work, we introduced a novel method to estimate dense depth maps from highly sparse measurements. The proposed interpolation uses a statistical model to obtain reduced rank signal subspaces which are learned by PCA. The dense depth maps are reconstructed as weighted linear combinations of these PCA basis signals. The necessary coefficients are determined by a maximum a-posteriori estimation approach which defuses the otherwise underdetermined problem.

The resulting depth maps yield a convincing coarse impression of the underlying depth structure. The numerical evaluation also shows that the estimated dense depth maps approximate the depth well on two challenging automotive datasets. Furthermore, we introduce uncertainty maps, a self-diagnosis tool that allows to find those areas where the interpolated / extrapolated depth is questionable. A drawback of these uncertainty maps are their relatively large computation costs. If the computation of the uncertainty map is skipped, our depth map interpolation scheme runs in real-time on a standard desktop computer.

A typical application case of our method is to provide a first initialization for a further densification step. For instance, a dense optical flow algorithm [8] converges faster utilizing a good initialization. This process flow is also claimed in [12]. Furthermore, sparse tracking algorithms [5], [3], [6] can be initialized with our dense depth in order to give good initializations for tracking further feature points. These application perspectives show that the proposed dense depth may be a valuable new component for real-time dense

reconstruction of the environment in context of autonomous driving.

REFERENCES

- [1] A. Geiger, P. Lenz, and R. Urtasun, "Are we ready for autonomous driving? the KITTI vision benchmark suite," in *Conference on Computer Vision and Pattern Recognition (CVPR)*, 2012, pp. 3354 – 3361.
- [2] A. Gaidon, Q. Wang, Y. Cabon, and E. Vig, "Virtual Worlds as Proxy for Multi-Object Tracking Analysis," in *Conference on Computer Vision and Pattern Recognition (CVPR)*, 2016, pp. 4340–4349.
- [3] J. Engel, T. Schöps, and D. Cremers, "LSD-SLAM: Large-Scale Direct Monocular SLAM," in *European Conference on Computer Vision (ECCV)*, 2014, pp. 834–849.
- [4] C. Forster, M. Pizzoli, and D. Scaramuzza, "SVO: Fast Semi-Direct Monocular Visual Odometry," in *International Conference on Robotics and Automation (ICRA)*, 2014, pp. 15–22.
- [5] N. Fanani, M. Ochs, H. Bradler, and R. Mester, "Keypoint trajectory estimation using propagation based tracking," in *Intelligent Vehicles Symposium (IV)*, 2016.
- [6] H. Bradler, M. Ochs, and R. Mester, "Joint epipolar tracking (JET): Simultaneous optimization of epipolar geometry and feature correspondences," in *Winter Conference on Applications of Computer Vision (WACV)*, 2017.
- [7] T. Brox, A. Bruhn, N. Papenberger, and J. Weickert, "High Accuracy Optical Flow Estimation Based on a Theory for Warping," in *European Conference on Computer Vision (ECCV)*, 2004, pp. 25–36.
- [8] B. K. P. Horn and B. G. Schunck, "Determining optical flow," *Artificial Intelligence*, vol. 17, pp. 185–203, 1981.
- [9] D. Gibson and M. Spann, "Robust optical flow estimation based on a sparse motion trajectory set," *Transactions on Image Processing*, vol. 12, no. 4, pp. 431–445, 2003.
- [10] C. Liu, J. Yuen, and A. Torralba, "SIFT Flow: Dense Correspondence across Scenes and Its Applications," *Transactions on Pattern Analysis and Machine Intelligence (PAMI)*, vol. 33, no. 5, pp. 978–994, 2011.
- [11] M. Leordeanu, A. Zanfir, and C. Sminchisescu, "Locally Affine Sparse-to-Dense Matching for Motion and Occlusion Estimation," in *International Conference on Computer Vision (ICCV)*, 2013, pp. 1721–1728.
- [12] J. Wulff and M. J. Black, "Efficient sparse-to-dense optical flow estimation using a learned basis and layers," in *Conference on Computer Vision and Pattern Recognition (CVPR)*, 2015, pp. 120–130.
- [13] R. Roberts, C. Potthast, and F. Dellaert, "Learning general optical flow subspaces for egomotion estimation and detection of motion anomalies," in *Conference on Computer Vision and Pattern Recognition (CVPR)*, 2009, pp. 57–64.
- [14] C. Herdtweck and C. Curio, "Experts of probabilistic flow subspaces for robust monocular odometry in urban areas," in *Intelligent Vehicles Symposium (IV)*, 2012, pp. 661–667.
- [15] A. Saxena, S. H. Chung, and A. Y. Ng, "Learning depth from single monocular images," in *Advances in Neural Information Processing Systems (NIPS)*, 2005, pp. 1161 – 1168.
- [16] D. Eigen, C. Puhrsch, and R. Fergus, "Depth Map Prediction from a Single Image using a Multi-Scale Deep Network," in *Advances in Neural Information Processing Systems (NIPS)*, 2014, pp. 2366–2374.
- [17] D. Eigen and R. Fergus, "Predicting Depth, Surface Normals and Semantic Labels with a Common Multi-scale Convolutional Architecture," in *International Conference on Computer Vision (ICCV)*, 2015, pp. 2650–2658.
- [18] R. Garg, V. K. B.G., G. Carneiro, and I. Reid, "Unsupervised CNN for Single View Depth Estimation: Geometry to the Rescue," in *European Conference on Computer Vision (ECCV)*, 2016, pp. 740–756.
- [19] M. Mancini, G. Costante, P. Valigi, T. A. Ciarfuglia, J. Delmerico, and D. Scaramuzza, "Towards Domain Independence for Learning-Based Monocular Depth Estimation," *Robotics and Automation Letters*, vol. PP, no. 99, pp. 1–1, 2017.
- [20] M. Cordts, M. Omran, S. Ramos, T. Rehfeld, M. Enzweiler, R. Benenson, U. Franke, S. Roth, and B. Schiele, "The Cityscapes Dataset for Semantic Urban Scene Understanding," in *Conference on Computer Vision and Pattern Recognition (CVPR)*, 2016, pp. 3213–3223.
- [21] H. Hirschmüller, "Stereo processing by semiglobal matching and mutual information," *Transactions on Pattern Analysis and Machine Intelligence (PAMI)*, vol. 30, no. 2, pp. 328–341, 2008.
- [22] J. Shi and C. Tomasi, "Good Features to Track," in *Conference on Computer Vision and Pattern Recognition (CVPR)*, 1994, pp. 593 – 600.